Supplementary

Effects of codoping on Tin Selenide nanomaterial to enhance thermoelectric performance above ambient temperature range

Pinaki Mandal[1], Soumyajit Maitra[2], Uday Kumar Ghorui[3], Prasenjit Chakraborty[1], Bibhutosh Adhikary[3] and Dipali Banerjee[1*]

[1]Department of Physics, Indian Institute of Engineering Science and Technology (IIEST), Shibpur, Howrah -711103, West Bengal, India

[2]School of Materials Science, Indian Association for the Cultivation of Science, Kolkata 700032, India

[3]Department of Chemistry, Indian Institute of Engineering Science and Technology (IIEST), Shibpur, Howrah-711103, West Bengal, India

*Email id: [1]dipalibanerjeebesu@gmail.com

Williamson-Hall plot

Average crystallite size (D) and lattice strain (ε) were calculated using Williamson-Hall plot (equation 1),

$$\beta\text{Cos}\theta = \frac{K\lambda}{D} + 4\varepsilon\,\text{Sin}\theta \qquad \ldots\ldots\ldots\ldots 1$$

where β is full width at half maxima (FWHM), K is the shape factor (0.94), and λ is the wavelength, respectively

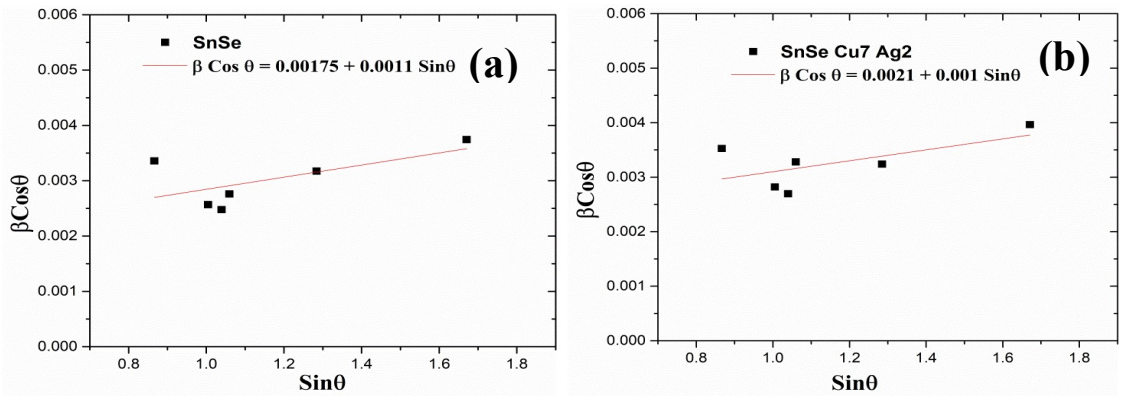

Figure S1 Williamson-Hall plots for pristine (a) SnSe and (b) SSCA-7-2

XPS Analysis

Figure S2 is the survey XPS spectrum of Cu/Ag codoped SnSe sample (SSCA-7-2). It reveals the presence of Cu 2p, Sn 3d, Ag 3d and Se 3d in codoped sample. C and O may come from ethylelediamine and small amount of tin oxide which may form during synthesis.

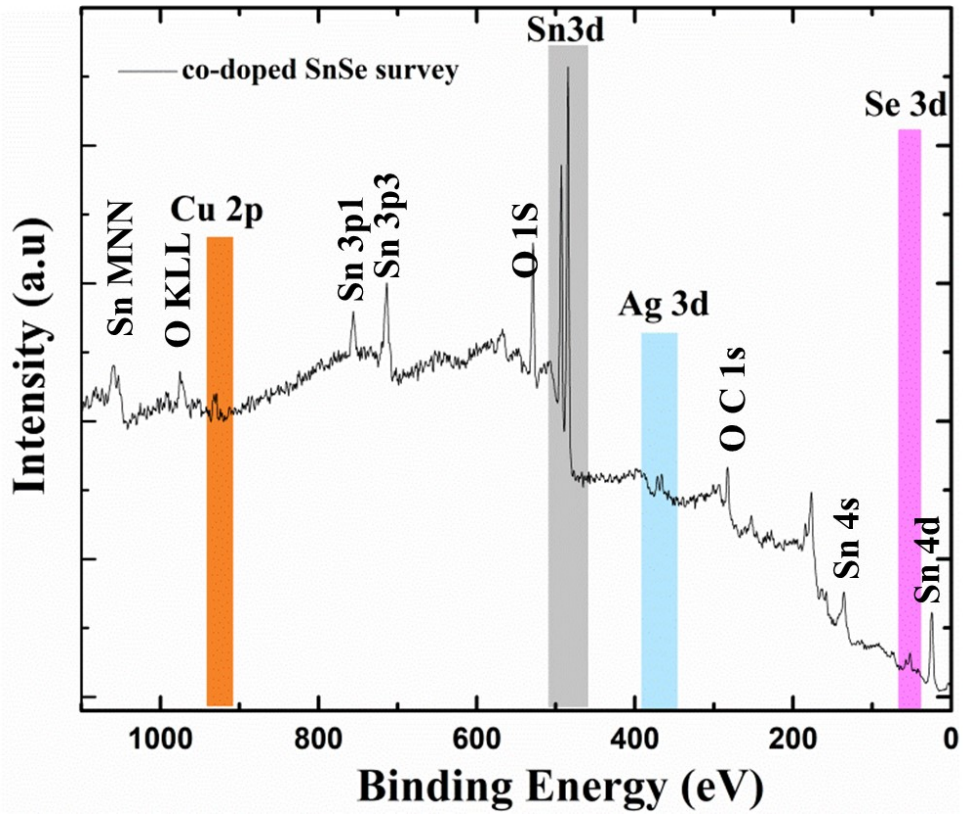

Figure S2 XPS survey scan for codoped SSCA-7-2

UV-Vis Analysis

UV-Vis spectra (shown in figure S3) were taken for the samples pure SnSe, Cu doped SnSe (SSCA-7-0) and Cu, Ag codoped SnSe (SSCA-7-2). Corresponding optical bandgaps (Eg) were calculated using Tauc relation[1] (equation 2)

$$\alpha h\nu = A_0[h\nu - E_g]^n \quad \text{.....2}$$

Where α, h, ν and A_0 are absorption coefficient, plank constant, frequency of radiation and constant respectively. Value of n depends on type of transition like ½, 2, 1/3 or 3 for allowed

direct, allowed indirect, forbidden direct, forbidden indirect transitions respectively. Obtained bandgap values are 1.05, 0.91 and 0.69 eV for pure SnSe, SSCA-7-0 and SSCA-7-2 respectively. Hence optical bandgap decreases for doped and codoped samples which is also observed in DFT results.

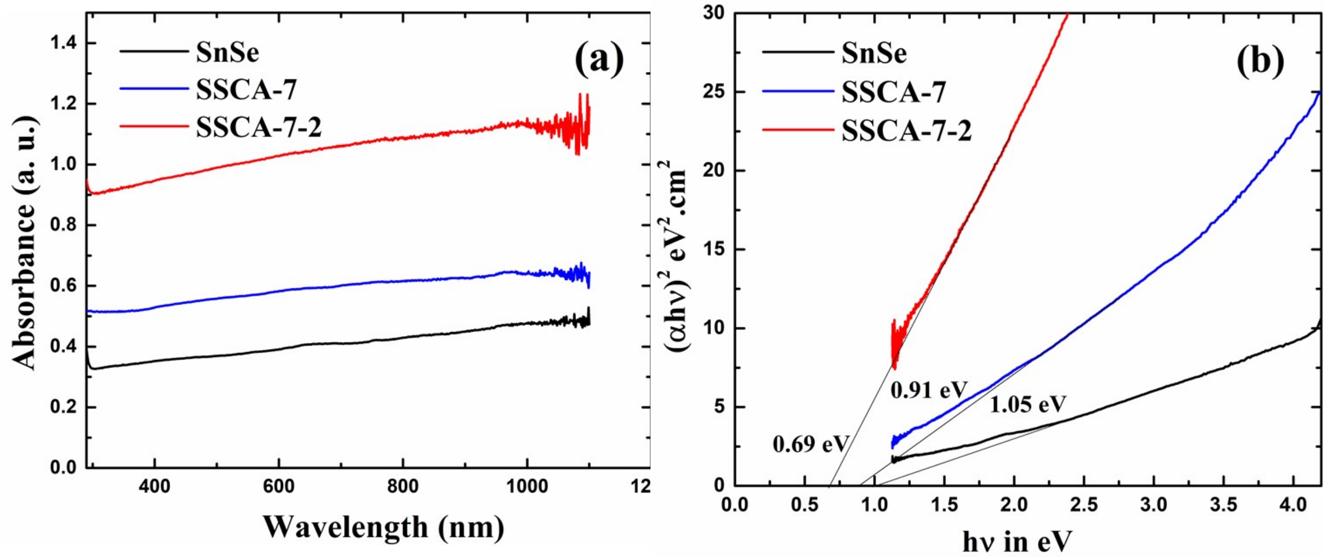

Figure S3 (a) UV-Vis spectra; (b) Tauc plot of pure SnSe, SSCA-7-0 and SSCA-7-2 respectively

Transport parameters

Carrier concentration has been calculated using Mott–Jones equation 3 (for M_e=0.9). Obtained values of carrier concentration and mobility are tabulated in Table S1 at room temperature along with recent similar works. Temperature variation of mobility for SSCA-7-2 has been shown in Figure S4

$$S = \frac{8\pi^2 k_B}{3eh^2} m^*_{DOS} T \left(\frac{\pi}{3n}\right)^{2/3} \quad \ldots\ldots\ldots\ldots\ldots\ldots\ldots\ldots\ldots\ldots\ldots\ldots \quad 3$$

Table S1 Carrier concentration and mobility calculated from Seebeck coefficient and reported values

Sample	n 10^{18} cm^{-3} from Hall measurement	n in 10^{18} cm^{-3} (Mott-Jones) (m*=0.9me)	Mobility (cm^2/VS) Hall measurement	Mobility (cm^2/VS) Calculated from Seebeck coefficint	Electrical conductivity S/cm	Reference
SnSe		8.28 5.32 (0.67 m_e)		0.0376	0.05	Present work
SSC-3		21.9 15.05(m*=0.7me) 9.38 (m*=0.51me)		0.0872	0.3	,,
SSC-7		32 22.15(m*=0.7me) 13.77 (m*=0.51me)		0.3019	1.54	,,
SSCA-7-1		48.9 16.15 (m*=0.43me)		0.5545	4.34	,,
SSCA-7-2		41.7 13.79 (m*=0.43me)		0.5261	3.51	,,
SSCA-7-3		37.9 12.51 (m*=0.43me)		0.5011	3.04	,,
SnSe SnSe 11.8 % Cu	0.18 3.44	6.78 13.71	160 57.2	4.3 14.12	4.7 31.6	[2]
SnSe SnSe 5% Ag	0.5 9	27.53 56.23	139 13	2.52 2.11	10.12 12.60	[3]
SnSe SnSe 1% Zn	0.15 0.2	8.9 (S=420μV/K) 5.4(S=585 μV/K)	56 30	0.32 0.57	0.46 0.50	[4]
SnSe $Sn_{0.94}Pb_{0.01}Se_{0.96}Te_{0.04}$	3.8 3.98	41.7(S=150 μV/K) 42.1(S=149 μV/K)	0.22 0.175	0.007 0.029	0.05 0.2	[5]
SnSe Na0.01(Sn1−0.05Pb0.05) 0.99Se	0.25 43.1	6.8 (S=502 μV/K) 41 (S=150 μV/K)	28 5.7	6.2	52 58	[6]

(from Hall Effect) at room temperature

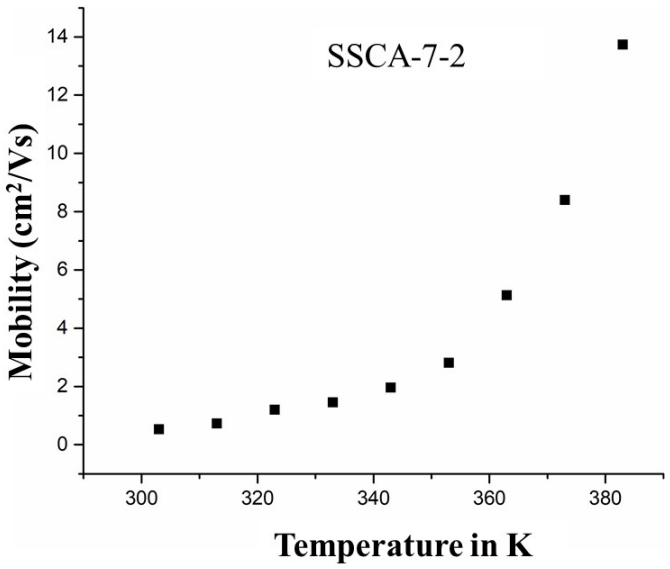

Figure S4 Temperature variation of mobility for SSCA-7-2

Computational Details

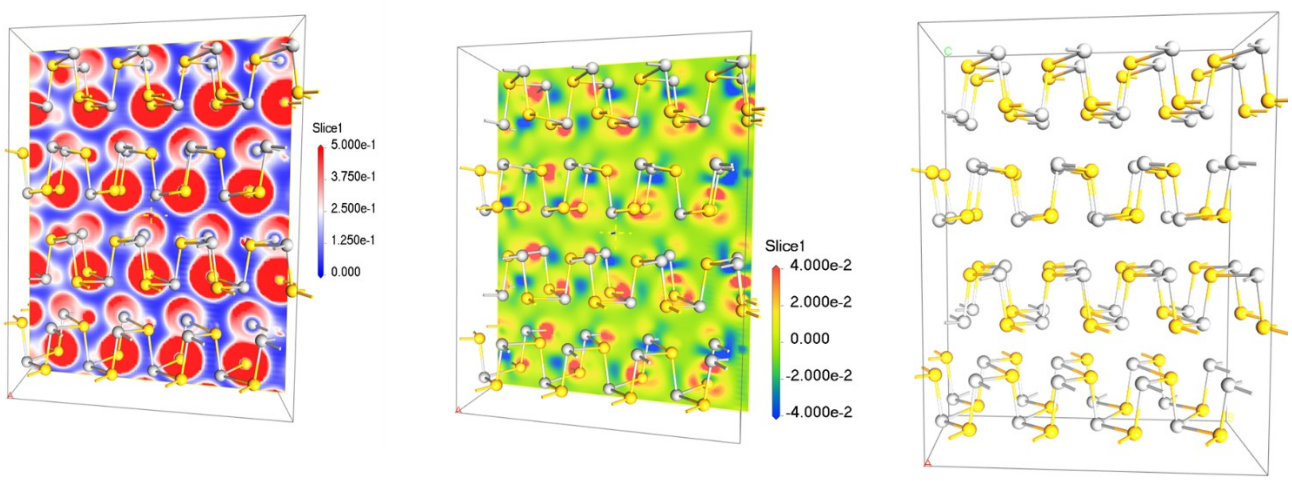

Figure S5 (a) ELF mapping of Cu-SnSe (b) EDD mapping of Cu-SnSe (c) Geometry optimized structure of SnSe supercell

DFT calculations were carried out using Quantum Expresso code using a Monkhorst Pack Scheme 9 × 9 × 3 k-point grid[7]. Spin-polarized DFT calculations were carried out with GGA exchange-correlationnd PBE type Ultrasoft pseudopotentials and Koelling-Harmon relativistic treatment[8,9]. DFT-D2 correction using Grimme Parameters for interlayer VdW interactions was taken into consideration since SnSe is a layered material. SCF cutoff was set at 1e-6 eV with a density mixing electronic minimizer scheme and a Pulay-type charge mixing scheme[9,10]. Geometry optimization was carried out using an LBFGS algorithm with energy cutoff set at 1e-6 eV, max force at 0.005 eV/Å, max stress at 0.01 GPa, and max displacement at 1e-5 Å[11,12] Phonon density of states and phonon dispersions were calculated using the Finite Displacement method for a single supercell, with convergence tolerance of 1e-6 eV and 0.005 1/Å dispersion grid separation[7].

References

(1) Mandal, P.; Maitra, S.; Chatterjee, M. J.; Chattopadhyaya, M.; Kargupta, K.; Banerjee, D. Polypyrrole-Bismuth Selenide (PPY-Bi2Se3) Composite-Thermoelectric Characterization and Effect of Nickel Doping. *Synthetic Metals*. 2022. https://doi.org/10.1016/j.synthmet.2022.117119.

(2) Shi, X.; Zheng, K.; Hong, M.; Liu, W.; Moshwan, R.; Wang, Y.; Qu, X.; Chen, Z. G.; Zou, J. Boosting the Thermoelectric Performance of P-Type Heavily Cu-Doped Polycrystalline SnSe: Via Inducing Intensive Crystal Imperfections and Defect Phonon Scattering. *Chem. Sci.* **2018**, *9* (37), 7376–7389. https://doi.org/10.1039/c8sc02397b.

(3) Chien, C. H.; Chang, C. C.; Chen, C. L.; Tseng, C. M.; Wu, Y. R.; Wu, M. K.; Lee, C. H.; Chen, Y. Y. Facile Chemical Synthesis and Enhanced Thermoelectric Properties of Ag Doped SnSe Nanocrystals. *RSC Adv.* **2017**, *7* (54), 34300–34306. https://doi.org/10.1039/c7ra05819e.

(4) Li, J. C.; Li, D.; Qin, X. Y.; Zhang, J. Enhanced Thermoelectric Performance of P-Type SnSe Doped with Zn. *Scr. Mater.* **2017**, *126*, 6–10. https://doi.org/10.1016/j.scriptamat.2016.08.009.

(5) Li, F.; Bo, L.; Zhang, R.; Liu, S.; Zhu, J.; Zuo, M.; Zhao, D. Enhanced Thermoelectric Properties of Te Doped Polycrystalline Sn0.94 Pb0.01 Se. *Nanomaterials* **2022**, *12* (9), 1–11. https://doi.org/10.3390/nano12091575.

(6) Lee, Y. K.; Ahn, K.; Cha, J.; Zhou, C.; Kim, H. S.; Choi, G.; Chae, S. I.; Park, J. H.; Cho, S. P.; Park, S. H.; Sung, Y. E.; Lee, W. B.; Hyeon, T.; Chung, I. Enhancing P-Type Thermoelectric Performances of Polycrystalline SnSe via Tuning Phase Transition Temperature. *J. Am. Chem. Soc.* **2017**, *139* (31), 10887–10896. https://doi.org/10.1021/jacs.7b05881.

(7) Opoku, F.; Govender, K. K.; Gertina, C.; Elizabeth, C.; Govender, P. P. (M = Zn and Cd) Heterostructures for Hydrogen Production : Insights from a DFT + U Study †. *Phys.Chem.Chem.Phys* **2017**, *19*, 28401–28413. https://doi.org/10.1039/c7cp04440b.

(8) Natarajan, K.; Chandiramouli, R. Exploring the Structural Stability and Electronic Properties of VS2 Nanostructures – a DFT Study. *J. Nano- Electron. Phys.* **2018**, *9* (February), 3–7. https://doi.org/10.21272/jnep.9(3).03008.

(9) Xu, Q.; Yang, G. M.; Zheng, W. T. DFT Calculation for Stability and Quantum Capacitance of MoS2 Monolayer-Based Electrode Materials. *Mater. Today Commun.* **2020**, *22*, 100772–100779. https://doi.org/10.1016/j.mtcomm.2019.100772.

(10) Maitra, S.; Pal, S.; Maitra, T.; Halder, S.; Roy, S. Solvothermal Etching-Assisted Phase and Morphology Tailoring in Highly Porous CuFe2O4Nanoflake Photocathodes for Solar Water Splitting. *Energy and Fuels* **2021**, *35* (17), 14087–14100. https://doi.org/10.1021/acs.energyfuels.1c02090.

(11) Ghosh, D.; Roy, K.; Maitra, S.; Kumar, P. Unravelling Rashba-Dresselhaus Splitting Assisted Magneto-Photoelectrochemical Water Splitting in Asymmetric MoSSe-GaN Heterostructures. *J. Phys. Chem. Lett.* **2022**, *13* (5), 1234–1240. https://doi.org/10.1021/acs.jpclett.1c04153.

(12) Roy, K.; Maitra, S.; Ghosh, D.; Kumar, P.; Devi, P. 2D-Heterostructure Assisted Activation of MoS2 Basal Plane for Enhanced Photoelectrochemical Hydrogen Evolution Reaction. *Chem. Eng. J.* **2022**, *435* (2), 134963. https://doi.org/https://doi.org/10.1016/j.cej.2022.134963.